



Surface equilibrium and dynamics for the adsorption of anionic dyes onto MnO₂/biomass micro-composite

Martins O. Omorogie, Michael T. Agbadaola, Abimbola M. Olatunde, Brigitte Helmreich & Jonathan O. Babalola

To cite this article: Martins O. Omorogie, Michael T. Agbadaola, Abimbola M. Olatunde, Brigitte Helmreich & Jonathan O. Babalola (2022) Surface equilibrium and dynamics for the adsorption of anionic dyes onto MnO₂/biomass micro-composite, Green Chemistry Letters and Reviews, 15:1, 49-58, DOI: [10.1080/17518253.2021.2018508](https://doi.org/10.1080/17518253.2021.2018508)

To link to this article: <https://doi.org/10.1080/17518253.2021.2018508>



© 2021 The Author(s). Published by Informa UK Limited, trading as Taylor & Francis Group



Published online: 24 Dec 2021.



Submit your article to this journal [↗](#)



Article views: 85



View related articles [↗](#)



View Crossmark data [↗](#)

Surface equilibrium and dynamics for the adsorption of anionic dyes onto MnO₂/biomass micro-composite

Martins O. Omorogie^{1b, a, b, c}, Michael T. Agbadaola^{d, e}, Abimbola M. Olatunde^d, Brigitte Helmreich^a and Jonathan O. Babalola^d

^aChair of Urban Water Systems Engineering, School of Engineering and Design, Technical University of Munich (TUM), Garching, Germany; ^bDepartment of Chemical Sciences, Faculty of Natural Sciences, Redeemer's University, Ede, Nigeria; ^cWater Science & Technology Research Unit, African Centre of Excellence for Water & Environmental Research (ACEWATER), Redeemer's University, Ede, Nigeria; ^dDepartment of Chemistry, Faculty of Science, University of Ibadan, Ibadan, Nigeria; ^eMolecular Biophysics, Technische Universität Kaiserslautern (TUK), Kaiserslautern, Germany

ABSTRACT

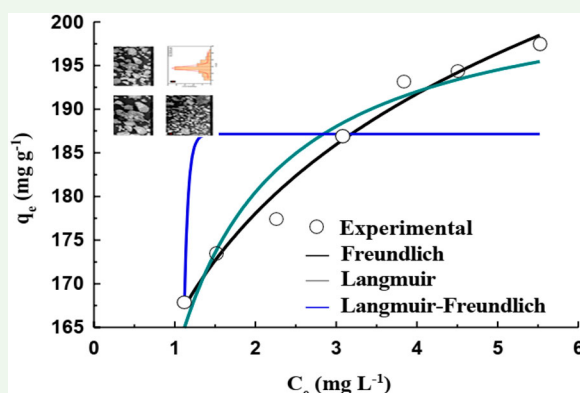
The properties of an adsorbent prepared from cost effective materials were discussed and analyzed in this research work. A ubiquitous biomass, *Terminalia ivorensis* biomass modified with MnO₂ (MTIB) was used for the adsorption of two anionic dyes (methyl orange (MO) and congo red (CR)). To adequately understand the viability of MTIB to adsorb MO and CR from contaminated water, it was characterized with some surface characterization techniques, which were bulk density, Boehm titration, pH point of zero charge, Fourier Transform Infra-Red and field emission-scanning electron microscopy. Surface characterization buttressed the experimental findings from multifarious data got from this research, which revealed that the major mechanisms for the adsorption of MO and CR onto MTIB were π - π stacking interaction and the adherence of these anionic dyes onto the functional moieties on the surface of MTIB. The experimental data most fit into the Langmuir-Freundlich equilibrium and Mixed-1,2-order kinetic models. The adsorption capacities, $q_{max,F}$ of MTIB for MO and CR were 81.32 and 92.84 mg g⁻¹ respectively. Desorption study showed that MTIB could be used as a suitable adsorbent to treat water contaminated with toxic anionic dyes.

ARTICLE HISTORY

Received 15 September 2021
Accepted 7 December 2021

KEYWORDS

Terminalia ivorensis/
manganese dioxide; micro-
composite; congo red;
methyl orange; adsorption



List of Abbreviations

Full Meanings

Terminalia ivorensis biomass modified with MnO₂
Ter/minalia ivorensis biomass (TIB)
Methyl Orange
Congo Red
World Health Organization

Abbreviations

MTIB
TIB
MO
CR
WHO
United Nations
Sustainable Development Goal
Advanced Oxidative Processes
Deoxyribonucleic Acid
Freundlich Model
Langmuir Model
Langmuir-Freundlich Model
Pseudo-First Order Model
Pseudo-Second Order Model

UN
SDG
AOPs
DNA
FM
LM
LFM
PFOM
PSOM

CONTACT Martins O. Omorogie  omorogiem@run.edu.ng, dromorogiemoon@gmail.com, mo.omorogie@tum.de  Chair of Urban Water Systems Engineering, School of Engineering and Design, Technical University of Munich (TUM), Am Coulombwall 3, Garching 85748, Germany; Department of Chemical Sciences, Faculty of Natural Sciences, Redeemer's University, P.M.B. 230, Ede 232101, Nigeria; Water Science & Technology Research Unit, African Centre of Excellence for Water & Environmental Research (ACEWATER), Redeemer's University, P.M.B. 230, Ede 232101, Nigeria

© 2021 The Author(s). Published by Informa UK Limited, trading as Taylor & Francis Group

This is an Open Access article distributed under the terms of the Creative Commons Attribution-NonCommercial License (<http://creativecommons.org/licenses/by-nc/4.0/>), which permits unrestricted non-commercial use, distribution, and reproduction in any medium, provided the original work is properly cited.

Mixed-1,2-Order Model	MOM
Bulk Density	BD
Boehm Titration	BT
pH Point of Zero Charge	pHPZC
Fourier Transform Infra-Red	FTIR
Field Emission-Scanning Electron Microscopy	FE-SEM
Gibb's Free Energy	ΔG°
Enthalpy Change	ΔH°
Entropy Change	ΔS°

1. Introduction

In recent years, the dearth of potable water, especially in developing nations of the world has been dreadful to the survival of humans. The lack of potable water is a threat to the continuous existence of humans worldwide. According to the World Health Organization (WHO) (1), One billion people in the world lack basic potable water service, and 15% of these people depend on surface water as their drinking water source. Over two billion people depend on water contaminated with feces and urine as their drinking water sources. This has led to an alarming increase in the mortality rate of infants in developing countries of the world. Water contaminated with feces and urine are harbingers and thriving grounds for various water-borne diseases, which include, diarrhea, cholera, dysentery, typhoid, polio, etc. (1). Contaminated water employed as a drinking water source has led to the death of over half a million people worldwide (especially in South America, Asia, and Africa), as a result of infections from enteric bacteria such as *Vibrio cholerae*, *Salmonella typhi*, *Escherichia coli*, among others.

In a bid to solve this global problem of serious concern, the WHO is working seriously to see that 50% of the population of the globe will live in water-stressed areas by 2025. In this vein, the United Nations (UN) has defined the availability of potable water to the world as its sixth sustainable development goal (SDG #6) by the year 2030 (1–4).

Researchers have risen in line with the objectives of the UN and WHO to terminate this challenge as water scientists are seeking varied techniques for treating contaminated water, to make them portable for the world populace. Some of these water treatment techniques are coagulation/flocculation (5, 6), membrane filtration (7, 8), advanced oxidative processes (AOPs) such as photocatalysis (9, 10), electrocatalysis (11, 12) and Fenton processes (13–15), adsorption (16–18), etc. Most of these techniques are expensive, consume high power, generate secondary sludge, and are unsustainable. Adsorption is a cost-effective and sustainable technique (16, 17) for treating contaminated water.

Industrial dyes reduce the impact of sunlight on aquatic plants during photosynthesis. Thus, the

chlorophyll in plants would produce fewer monosaccharides to drive metabolic processes. This will influence the survival of plants negatively in the aquatic environment. Industrial dyes form their intermediate analogs and aromatic amines that are deleterious to the aquatic habitat and humans due to their carcinogenicity (high risk of cancer occurrence), mutagenicity (negative effects on deoxyribonucleic acid (DNA) in the cells), and toxicity, which include the bladder cancer, blood cancer, bone marrow cancer, fertility difficulties, dizziness, the appearance of hives, allergies, asthma, hyperactivity, irritability, dermatitis, and angioedema, skin irritation, jaundice, cyanosis, burns vomiting, diarrhea, nausea blood, and bone marrow cancer, mental retardation, fertility challenges, to mention a few (19–21).

The use of biological-based materials as sources of cheap adsorbents has some drawbacks. These drawbacks are mainly low mass-volume ratio, low bulk density, and decomposition in aqueous solutions at elevated temperatures over a period of time. The novelty of this research work is based on fact that the functionalization of *Terminalia ivorensis* biomass with MnO_2 reduced these drawbacks. This research hinges on the application of MnO_2 functionalized *Terminalia ivorensis* biomass (MTIB) for the removal of anionic dyes from aqueous solutions.

2. Materials and methodology

2.1. Chemical reagents

The chemical reagents used in this research were manganese oxalate monohydrate ($C_2O_4 \cdot H_2O$)Mn (>99% purity), HNO_3 (70% purity), HCl (>37.5% purity), H_2SO_4 (>97% purity), NaOH (>80% purity), $MnSO_4 \cdot H_2O$ (>98.5% purity), anionic dyes [Methyl orange (MO) and Congo red (CR)]. They were all obtained from Sigma-Aldrich and used for this research work without further purification.

2.2. Preparation of stock solutions

A 1 g L^{-1} of stock solutions of MO and CR were prepared by dissolving accurately weighed amounts of these anionic dyes in distilled water, and diluting them to various working concentrations. Adsorption studies were conducted by optimizing various operating parameters such as pH, adsorbent dose, initial dye concentrations, agitation time and temperature. All experiments were performed in triplicate and standard deviation of ± 0.25 .

2.3. Preparations of modified biomass

The *Terminalia ivorensis* biomass (TIB) was collected from Botanical Garden, University of Ibadan, Ibadan (7.3775°

N, 3.9470° E), Nigeria, and identified at the Department of Botany, University of Ibadan, Ibadan, Nigeria. The sample was washed with distilled water, air-dried for four weeks, and pulverized. The pulverized biomass was oven-dried for 1 h at 373 K and sieved with a 250 µm mesh sieve. The sieved biomass functionalized with MnO₂ was prepared using a published protocol (22). Briefly, MnO₂ was prepared by co-precipitation method using Manganese salts of two different anions (Manganese sulphate and Manganese oxalate). Both salts of equal concentration (0.2 M) were mixed under continuous stirring for 1 h at 373 K. Then, 0.1 M NaOH was added intermittently until a pH of 12.0 was achieved (23). The reaction mixture was further stirred for 3 h, followed by the addition of 10 g of pulverized TIB. The black MnO₂-functionalized TIB (MTIB) slurry formed was filtered and washed twice with warm distilled water, so as to remove unreacted salts. This MTIB slurry was oven-dried overnight at 373 K and kept in an airtight container for future use.

2.4. Adsorption studies

Adsorption studies were observed by the uptake of MO and CR onto MTIB using the batch-adsorption technique. All experiments were performed in triplicate and the averages were used in each case. For each experiment, 25 mL of 100 mg L⁻¹ anionic dye solution of MO and CR was measured into separate plastic bottles containing a known amount of MTIB. The volume and concentration of the dyes were kept constant for every experiment except where otherwise stated. These bottles were tightly corked and agitated in a thermostatic water bath shaker (Gallenkamp, UK) at 125 rpm for 2 h. The effect of pH (2.0 to 12.0), adsorbent dosages (10 to 1000 mg), agitation time (0.5 to 120 min), initial dye concentrations (20 to 200 mg L⁻¹) and temperatures (298 to 328 K) was studied. Desorption kinetic experiments were performed using 0.1 M HCl and 0.1 M HNO₃ to ascertain the rate of regeneration of MO and CR from the surface of MTIB from 0.5 to 120 min.

2.5. Experimental data modeling and analysis

Aliquots were removed from the thermostatic water bath shaker at varied time intervals for equilibrium, kinetic and thermodynamic analyses of experimental data.

In all experiments, the adsorbent was separated from the adsorbate by centrifugation, using a centrifuge (Hitachi, China) at 5000 rpm for 10 min at room temperature. Each supernatant was analyzed using a double-

beam UV/Visible Spectrophotometer (Jasco, Japan) at a maximum wavelength of absorption (464 nm for MO and 498 nm for CR). The amounts of solutes adsorbed, q_e , by MTIB (mg g⁻¹) was calculated using the mass balance equation given as

$$q_e = \int_{i=1}^n \left\{ (C_o - C_e) \cdot \frac{V}{W} \right\} \quad (1)$$

The quasi-Newton least square algorithm in KyPlot software 2.0 model (KyensLab Inc., Tokyo, Japan) was used to fit the experimental data into multifarious equilibrium, kinetic and thermodynamic equations, which are

$$q_e = K_f C_e^{1/n} \quad \text{Freundlich model (FM)} \quad (2)$$

$$q_e = \frac{q_{\max L} K_L C_e}{1 + K_L C_e} \quad \text{Langmuir model (LM)} \quad (3)$$

$$q_e = \frac{K_{LF} C_e^{n_{LF}}}{1 + (q_{\max LF} C_e)^{n_{LF}}} \quad (4)$$

Langmuir-Freundlich model (LFM)

$$q_t = q_e (1 - e^{-k_1 t}) \quad (5)$$

Pseudo-First Order model (PFOM)

$$q_t = \frac{k_2 q_e^2 t}{1 + k_2 q_e t} \quad (6)$$

Pseudo-Second Order model (PSOM)

$$q_t = q_e \left(\frac{1 - e^{-k_{1,2} t}}{1 - \eta e^{-k_{1,2} t}} \right) \quad (7)$$

Mixed-1, 2-Order model (MOM)

$$\ln \left(\frac{k_2}{T} \right) = \ln \left(\frac{k}{h} \right) - \left(\frac{\Delta H^\circ}{RT} \right) + \left(\frac{\Delta S^\circ}{R} \right) \quad (8)$$

Eyring model

where k_f , n , K_L , $q_{\max L}$, q_t , k_1 , k_2 , ΔS° , ΔH° , R , T , $q_{\max LF}$, n_{LF} , K_{LF} , $k_{1,2}$, η , k and h , are Freundlich constant (mg g⁻¹) (L mg⁻¹)^{1/n}, an empirical constant that represents the adsorption affinity, Langmuir adsorption constant (L mg⁻¹), q_e for a complete monolayer (mg g⁻¹), amounts of solute ions adsorbed at time t (min) by MTIB (mg g⁻¹), pseudo-first order rate constant (min⁻¹), pseudo-second order rate constant (g mg⁻¹ min⁻¹), entropy change (J mol⁻¹ K⁻¹), enthalpy change (J mol⁻¹), universal gas constant (8.314 J mol⁻¹ K⁻¹), absolute temperature (K), Langmuir Freundlich equilibrium adsorption capacity (mg g⁻¹), Langmuir-Freundlich constant for adsorption affinity, Langmuir-Freundlich constant (mg g⁻¹) (L mg⁻¹)^{1/n}, Mixed-1,2-order rate constant (min⁻¹), Mixed-1,2-order exponent (min⁻¹), Boltzmann constant (1.381 × 10⁻²³ J K⁻¹) and Planck constant (6.626 × 10⁻³⁴ J s) respectively.

2.6. Surface characterization of MTIB

Surface characterization of MTIB was done using bulk density (BD), Boehm titration (BT), pH point of zero charge (pHPZC), Fourier Transform Infra-Red (FTIR), and field emission-scanning electron microscopy (FE-SEM).

3. Results and discussion

3.1. BD, BT, pHPZC, FTIR and FE-SEM of MTIB

The bulk density of MTIB was 0.261 g cm^{-3} . The results from Boehm titration indicate 1.425 and $0.825 \text{ mmol g}^{-1}$ of acidic and basic functional moieties on the surface of MTIB respectively. In overall, MTIB comprises more positive than negative charges, and this reflects the fast uptake of these anionic dyes (MO and CR) at different experimental conditions.

The pHPZC (isoelectric pH) of the surface of MTIB was 7.98 (see Figure 1). It was expected therefore that the adsorption of MO and CR was greatly enhanced at low pH values due to their anionic form. At $\text{pH} < \text{pHPZC}$ and $\text{pH} > \text{pHPZC}$, the surface of MTIB has more positive and negative charges respectively. This means that MO and CR were more adsorbed by MTIB at $\text{pH} < \text{pHPZC}$ due to their anionic form (10,16). The results from pH studies and other previous reports in the literature confirmed that maximum adsorption of MO and CR was achieved at pH 2.0 (20,21).

Figure 2 shows the FTIR spectrum of MTIB, which reflected distinct peaks of aliphatic and aromatic C–H stretch, aromatic hydroxyl stretch, aromatic amine stretch, aromatic sulphhydryl stretch, aromatic carbonyl bend, and Mn–O stretch at 3785, 3745, 3441, 2329,

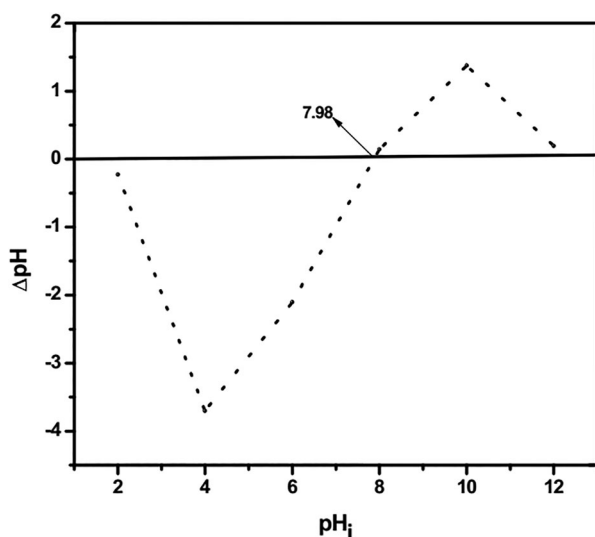


Figure 1. The pHPZC of MTIB.

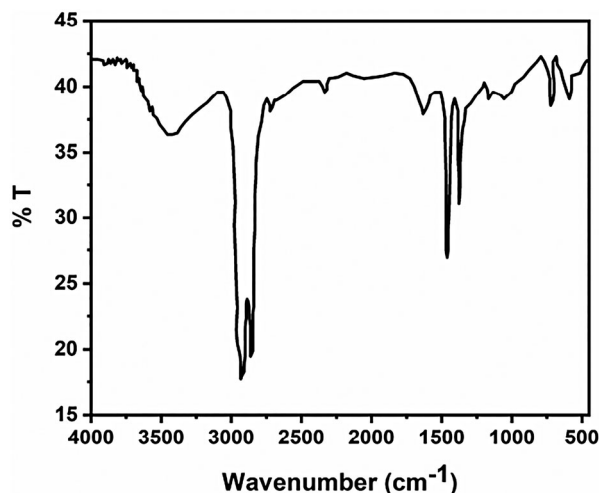


Figure 2. The FTIR spectrum of MTIB.

721.51, and 519.76 cm^{-1} respectively. The aromatic moieties in MTIB are responsible for a certain degree of aromatization, leading to high electron cloud densities, which enhance the adsorption of MO and CR onto MTIB by π - π stacking interactive mechanism (10, 16, 23).

Figure 3(a–c) show the FE-SEM micrographs of MTIB at 1500 \times , 1000 \times , 510 \times , and its particle size distribution (3d). These micrographs show large clogs of agglomerated particles that are irregularly scattered. The cell wall of the biomass contains lignocelluloses, which are probably lined with the micro-particles of MnO_2 (24, 25). Although, these are not visible on the FE-SEM micrographs. From Figure 3d, the particle size analysis indicated that the average diameter of the particles is $35.43 \mu\text{m}$.

3.2. Effects of pH, initial dye concentrations, adsorbent dose, agitation time, and temperature

The relevance of pH in adsorption studies cannot be over-emphasized. The solution chemistry of adsorbates strongly determines the adsorption capacities of charged ions onto the surfaces of the adsorbents. Figure 4 indicates that there is no clear trend between the adsorption of MO and CR by MTIB with increasing pH. Adsorption was maximum for MO and CR at pH 2.0 with adsorption capacities of 97.52 and 96.56 mg g^{-1} respectively after which adsorption decreases steadily to a minimum capacity of 55.65 mg g^{-1} at pH 10 for MO, and 38.32 mg g^{-1} at pH 8.0 for CR before a steady increase was observed again up to pH 12.0 for both dyes. The decrease in the adsorption capacity may be due to decrease in the proton density on the surface of MTIB, thereby decreasing the static attraction and increasing the repulsion of the

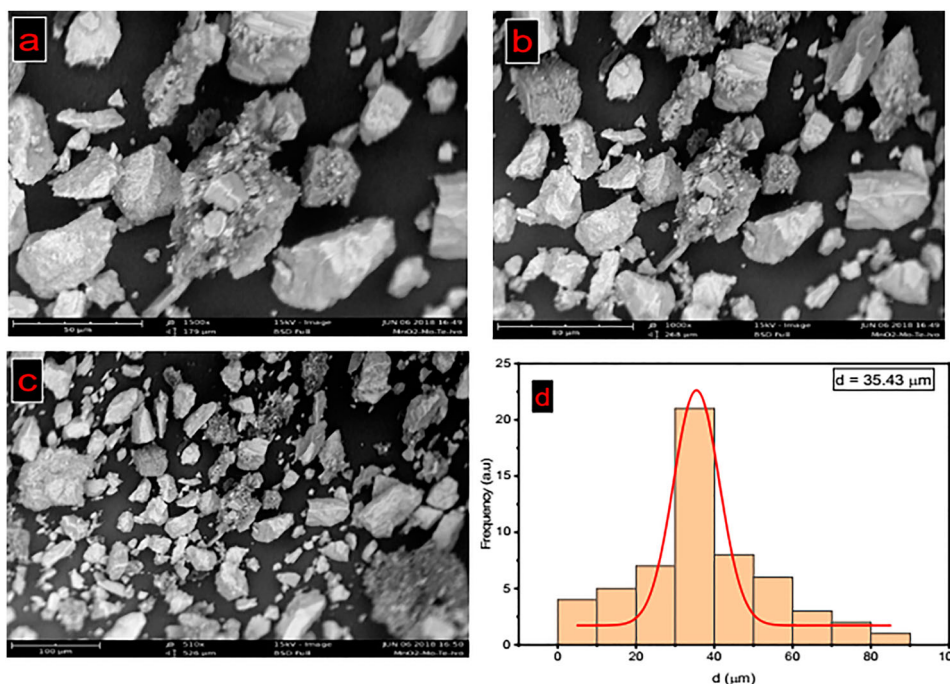


Figure 3. (a–c) The FE-SEM images, and (d) particle size distribution of MTIB.

adsorption of the anionic dyes onto the MTIB surface. The fast increase in the adsorption capacity observed between pH 8.0 and pH 12.0 may be due to charge stabilization on the surface of the adsorbent, which decreases the adsorbent–adsorbate repulsion, thereby increasing the amounts of dyes adsorbed on the surface of MTIB.

The adsorption of MO and CR onto MTIB increased with an increase in the initial concentrations of both dyes. The MO and CR molecules occupied the active sites of MTIB in rapid successions until there were no more active sites for MO and CR molecules to occupy. At equilibrium, which was the point of saturation of the active sites on the surface of MTIB with these dye

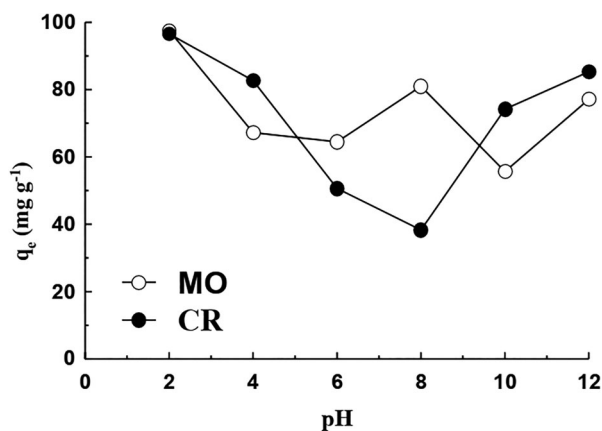


Figure 4. The adsorption of MO and CR onto MTIB at different pH.

molecules, MTIB stopped further adsorption of MO and CR on its surface (26, 27).

Figure 5 shows that as the adsorbent dose study, which indicated that the mass of MTIB increased from 10 to 1000 mg. The adsorption of MO and CR decreased drastically from 229.61 to 2.37 mg g⁻¹ and 249.8 to 2.42 mg g⁻¹ respectively. This sharp decrease was as a result of the clogging and agglomeration/aggregation of MTIB particles as its mass increases. This phenomenon tends to elongate the diffusion paths for the adsorption of MO and CR onto MTIB (18, 27, 28).

The amount of solutes adsorbed by MTIB is dependent on the resident time that the adsorption process occurred. Therefore, the resident time for adsorbate–

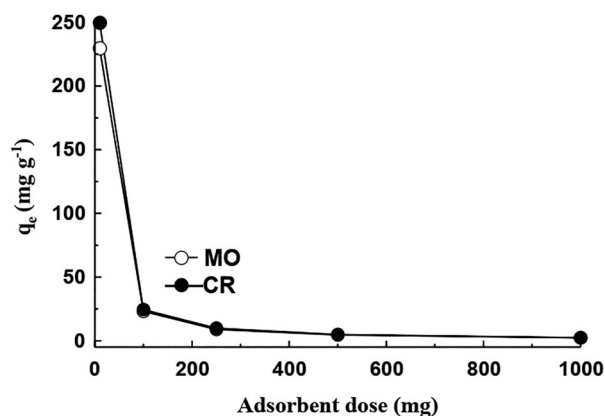


Figure 5. The adsorption of MO and CR onto MTIB at different adsorbent doses.

adsorbent interaction is significant in determining the adsorption capacity of an adsorbent, especially at the early stage of adsorption. This was observed for the adsorption of MO and CR onto MTIB, which was rapid within 1 h after adsorption process had begun. After 1 h, the adsorption of MO and CR by MTIB undergo a sharp decline and remain stable. The stability in this adsorption process was achieved due to the absence of unoccupied/vacant active sites for MO and CR to occupy even with increased resident time (27, 28).

The collision frequency and kinetic energy generated because of the adsorbate–adsorbent interaction increased as the temperature increased. It was observed that from 30 s to 1 h, the adsorption of MO by MTIB increased from 28 to 77 mg g⁻¹, 37 to 94.90 mg g⁻¹ and 45 to 114.80 mg g⁻¹ at 298, 313, and 328 K, respectively. Similarly, from 30 s to 1 h, the adsorption of CR by MTIB increased from 42 to 94 mg g⁻¹, 51 to 107 mg g⁻¹ and 60 to 118 mg g⁻¹ at 298, 313, and 328 K, respectively. After 1 h, the adsorption of MO and CR by MTIB drastically decreased at all temperatures due to the absence of vacant active sites (17, 18, 26).

3.3. Adsorption equilibrium, kinetics, and thermodynamics

To better understand the adsorption process, the uptake of MO and CR by MTIB was critically analyzed for its adsorption capacity at high initial concentrations. Adsorption equilibrium plays a significant role in understanding the adsorption capacities of adsorbents as solute concentration increases. Therefore, the adsorption equilibrium data were fit into two-parameters (Freundlich (29), Langmuir (30)), and three-parameters (Langmuir-Freundlich (28, 31)) isotherm models (Equations (2) to (4)). The experimental data for the adsorption of MO and CR onto MTIB indicated that the Langmuir-Freundlich model best described this adsorption process, which was interplay of both homogeneous and heterogeneous active sites, which were responsible for monolayer and multilayer coverage of the surface of MTIB by MO and CR. This implies that the surface of MTIB comprises different active sites that interacted with MO and CR during the equilibrium process. Table 1 shows that the adsorption capacities, $q_{max,LF}$ of MTIB for MO and CR, were 81.32 and 92.84 mg g⁻¹ respectively, and Figures 6 and 7 show the quantity, q_e (mg g⁻¹) of MO and CR adsorbed at equilibrium concentration, C_e (mg L⁻¹).

Adsorption kinetic models relate the rate at which the solutes migrate to the active sites on the surfaces of adsorbents as a representation of the solutes uptake

Table 1. Non-linear equilibrium parameters for the adsorption of MO and CR by MTIB.

Models	MO	CR
FM		
K_F (mg g ⁻¹)(L mg ⁻¹) ^{1/n}	1.241	1.347
1/n	0.151	0.599
r^2	0.993	0.991
LM		
$q_{max,L}$ (mg g ⁻¹)	79.034	89.843
K_L (L mg ⁻¹)	0.457	0.491
r^2	0.972	0.968
LFM		
$q_{max,LF}$ (mg g ⁻¹)	81.324	92.847
K_{LF} (L mg ⁻¹)	0.414	0.427
n_{LF}	14.043	9.564
r^2	0.996	0.997

with time. The dynamics at which the adsorbates access and interact with the active sites on the surfaces of adsorbents give a striking insight into their applicability. Essentially, adsorbate–adsorbent interaction is only complete when there are (1) steady migration of solutes from the bulk solutions into the film or boundary layers of adsorbents, (2) further migration of these solutes from the boundary layers of adsorbents into the intra-particles and pores of the adsorbents (17, 18, 32). Therefore, kinetic models greatly support the pore migration of solutes into active sites of adsorbents (32). The adsorption kinetic data were fit into two-parameters (Pseudo-first order, Pseudo-second order), and three-parameters (Mixed-1,2-order) kinetic models (Equations (5) to (7)). Table 2 shows that the experimental data for the adsorption of MO and CR onto MTIB indicated that the mixed-1,2-order model best described this adsorption kinetic process. From the mixed-1,2-order model in Table 2, the amounts of MO and CR adsorbed by MTIB were 78.93 to 95.11 mg g⁻¹ at 298 to 333 K and 101.32 to 125.26 mg g⁻¹ at 298 to 333 K, respectively, and

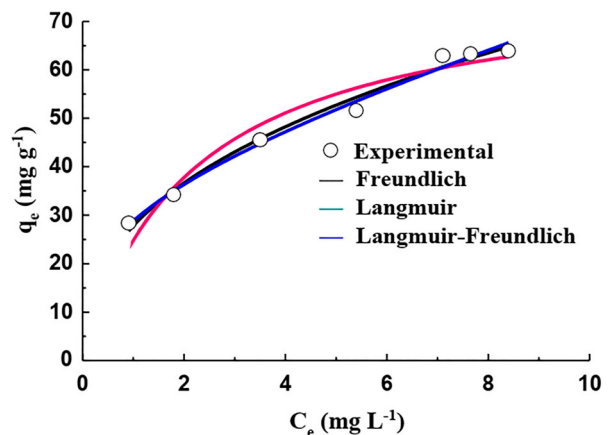


Figure 6. Non-linear adsorption isotherms for the amounts, q_e (mg g⁻¹) for MO adsorbed by MTIB.

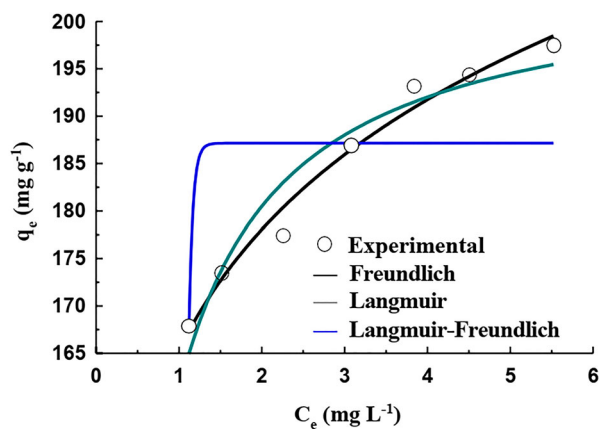


Figure 7. Non-linear adsorption isotherms for the amounts, q_e (mg g^{-1}) for CR adsorbed by MTIB.

Figures 8 and 9 show the quantity, q_e (mg g^{-1}) of MO and CR adsorbed at equilibrium concentration, C_e (mg L^{-1}).

Table 3 succinctly describes the thermodynamics results (calculated with Equation (8)) for the adsorption process. The adsorption was non-spontaneous at 298 K with the Gibb's free energy change values (ΔG°) of $+4.28 \text{ kJ mol}^{-1}$ and $+13.88 \text{ kJ mol}^{-1}$ for MO and CR, respectively. The increase in temperature from 298 to 313 K and 328 K made (ΔG°) to be negative, indicating spontaneity. It is important to note that MTIB was at its best at elevated temperatures. The enthalpy change (ΔH°) and entropy change (ΔS°) were positive for both dyes. This implies that the adsorption process was endothermic with heat energy absorbed from the surroundings and a corresponding increase in the chaos at the adsorbate-adsorbent interface. This led to an increase in the amounts of MO and CR adsorbed onto MTIB. The ΔH° value for the adsorption of CR was higher than that of MO. This explains the increased adsorption capacity of CR onto MTIB compared to that of MO.

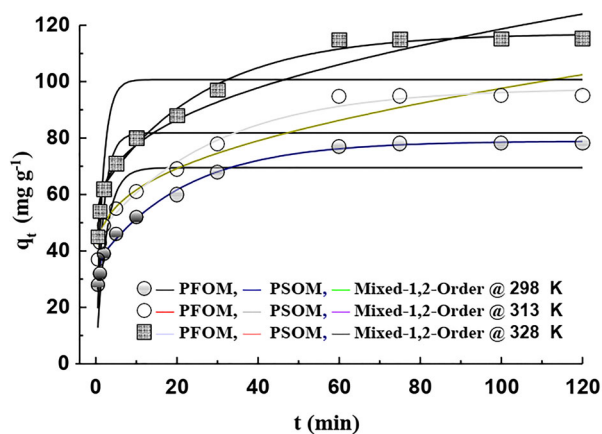


Figure 8. Non-linear kinetic fits for the amounts, q_t (mg g^{-1}) at time t (min) for MO adsorbed by MTIB.

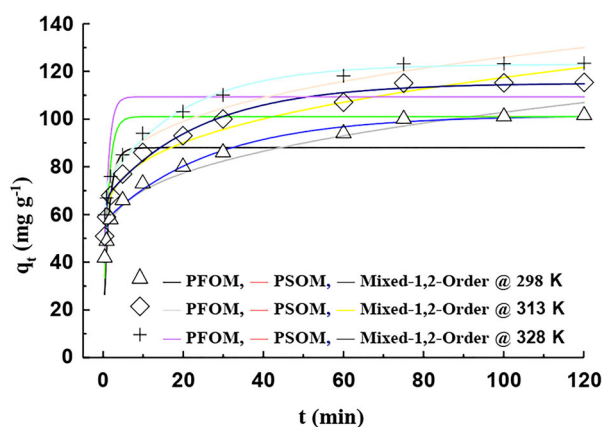


Figure 9. Non-linear kinetic fits for the amounts, q_t (mg g^{-1}) at time t (min) for CR adsorbed by MTIB.

3.4. Regeneration of MTIB

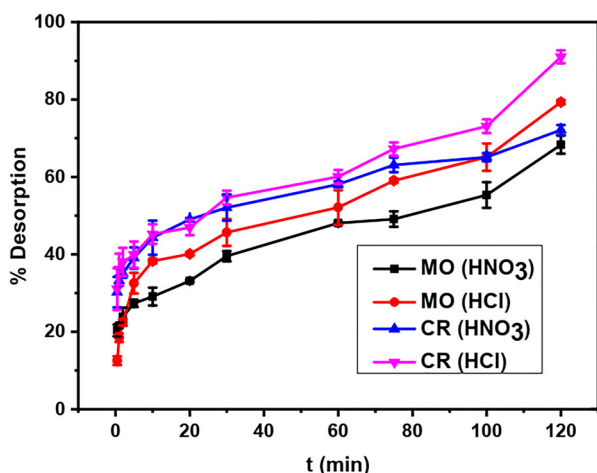
Adsorbent reusability is an essential factor in considering its viability when subjected to industrial applications. In this research work, 0.1 M HCl and 0.1 M HNO_3 were used to desorb MO and CR from 0.5 to 120 min (calculated with Equation (9)).

Table 2. Non-linear kinetic parameters for the adsorption of MO and CR by MTIB.

Model	MO			CR		
	298 K	313 K	328 K	298 K	313 K	328 K
PFOM						
q_e (mg g^{-1})	69.481	72.779	83.346	87.987	100.951	107.121
k_1 (min^{-1})	0.408	0.603	0.831	0.207	0.225	0.383
r^2	0.834	0.801	0.761	0.815	0.887	0.897
PSOM						
q_e (mg g^{-1})	76.771	79.437	88.356	90.321	109.849	113.835
k_2 ($\text{g mg}^{-1} \text{min}^{-1}$)	0.146	0.197	0.281	0.586	0.588	0.752
r^2	0.971	0.978	0.981	0.982	0.983	0.985
MOM						
q_e (mg g^{-1})	78.933	87.651	95.111	101.321	114.993	125.256
$k_{1,2}$ ($\text{g mg}^{-1} \text{min}^{-1}$)	0.387	0.555	0.649	0.037	0.049	0.057
η	0.046	0.035	0.031	0.006	0.003	0.002
r^2	0.996	0.997	0.998	0.994	0.996	0.998

Table 3. Thermodynamic data for the adsorption of MO and CR onto MTIB.

Dyes	ΔG° (kJ mol ⁻¹)			ΔH° (kJ mol ⁻¹)	ΔS° (kJ mol ⁻¹)
	298 K	313 K	328 K		
MO	+4.28	-41.38	-79.31	+825.11	+2.79
CR	+13.88	-29.53	-58.31	+1012.07	+2.35

**Figure 10.** The desorption kinetics of MO and CR from MTIB.

The amounts of MO desorbed from the surface of MTIB when 0.1 M HCl and 0.1M HNO₃ were used as desorbing agents from 0.5 to 120 min were 12.55% to 79.32% and 20.35% to 68.33% respectively.

Similarly, the amounts of CR desorbed from the surface of MTIB when 0.1 M HCl and 0.1M HNO₃ were used as desorbing agents from 0.5 to 120 min were 31.02% to 91.03% and 30.23% to 72.12% respectively. This indicates that more CR molecules than MO molecules were desorbed from the surface of MTIB. The highest desorption rates for MO and CR from the surface of MTIB were achieved with 0.1 M HCl after 2 h. Figure 10 shows the desorption kinetics of MO and CR from MTIB. The equation below was used to calculate the percentage desorption of MO and CR. Table 4 comprises adsorption capacities of multifarious materials for MO and CR in literature.

$$\% \text{ Desorption} = \frac{\text{Amount desorbed}}{\text{Amount adsorbed}} \times 100 \quad (9)$$

4. Conclusion

The adsorption of MO and CR by MTIB was studied under various conditions, which include pH, initial dye concentrations, adsorbent dose, agitation time, and temperature. The experimental data fit best into the Langmuir-Freundlich equilibrium and Mixed-1,2-order kinetic models. The adsorption capacities of MTIB for MO and

Table 4. Published adsorption capacities of various materials for MO and CR.

Adsorbents	$q_{\text{max},F}$ (mg g ⁻¹)		$q_{\text{max},F}$ (mg g ⁻¹)	
	CR	References	MO	References
<i>Pentaclethra macrophylla</i> bark	157.23	(33)		
<i>Malacantha alnifolia</i> bark	800	(33)		
<i>Cedrela odorata</i> seed waste	128.84	(28)	68.23	(28)
<i>Parkia biglobosa</i> cellulosic extract	288.18	(34)		
<i>Parkia biglobosa</i> seed waste	266.67	(34)		
<i>Eichhornia crassipes</i> roots	1.58	(35)		
Chitosan			34.83	(36)
Calcined Lapindo volcanic mud			333.30	(37)
<i>Phragmites australis</i> activated carbon			238.10	(38)
γ -Fe ₂ O ₃ /SiO ₂ /chitosan composite			34.29	(39)
MTIB	81.31	This study	92.84	This study

CR were 81.32 and 92.84 mg g⁻¹ respectively. Bulk density (BD), Boehm titration (BT), pHPZC, FTIR, and FE-SEM were employed to characterize the surface of MTIB. These characterization tools for MTIB revealed that surface functional moieties were responsible for the uptake of these anionic dyes. Also, desorption studies revealed the reusability potential of MTIB for applications in water treatment.

Acknowledgements

Dr. Martins O. Omorogie acknowledges the Department of Chemical Sciences, Faculty of Natural Sciences, Redeemer's University (RUN), Ede, Osun State, Nigeria for a short postdoctoral research leave. Dr. Omorogie thanks Prof. Brigitte Helmreich and the Chair of Urban Water Systems Engineering, School of Engineering and Design TUM, Germany for all technical supports. Prof. Babalola and Mr. Michael Agbadaola are grateful to the Department of Chemistry, University of Ibadan, Ibadan, Nigeria for assistance.

Authors' contributions

Mr. Michael T. Agbadaola: Generated some of the experimental data in the laboratory, as part of his MSc research. Wrote the original draft of this manuscript and analyzed part of the data in this manuscript.

Dr. Martins O. Omorogie: Conceptualized the idea in this manuscript, supervised the writing and the revision of this original draft of this manuscript, wrote this manuscript, reviewed, revised, edited and analyzed the data in this manuscript. Supervised this work, as part of Mr. Michael T. Agbadaola's MSc research project.

Dr. Abimbola M. Olatunde: Co-supervised this work, as part of Mr. Michael T. Agbadaola's MSc research project.

Prof. Dr. Brigitte Helmreich: Edited the original draft of this manuscript, revised this original draft of this manuscript, reviewed, revised and analyzed the data in this manuscript.

Prof. Jonathan O. Babalola: Supervised the revision of this original draft of this manuscript, reviewed, edited and analyzed the data in this manuscript. Supervised this work, as part of Mr. Michael T. Agbadaola's MSc research project.

Consent to publish

All the authors of this manuscript have given their consent for it to be published.

Disclosure statement

No potential conflict of interest was reported by the author(s).

Funding

The authors thank the Deutsche Forschungsgemeinschaft-The World Academy of Sciences (DFG-TWAS) for the financial support (scholarship) granted to Dr. Martins O. Omorogie (HE-2413/7-1).

ORCID

Martins O. Omorogie  <http://orcid.org/0000-0001-9697-2960>

References

- [1] Organization, W.H. National Systems to Support Drinking-Water: Sanitation and Hygiene: Global Status Report 2019: UN-Water Global Analysis and Assessment of Sanitation and Drinking-Water: GLAAS 2019 Report, 2019.
- [2] Grandjean, A.C. Water Requirements, Impinging Factors, and Recommended Intakes: Nutrients in Drinking Water. *2005*, 25.
- [3] Pal, M.; Ayele, Y.; Hadush, M.; Panigrahi, S.; Jadhav, V. Public Health Hazards Due to Unsafe Drinking Water. *Air. Water Borne Dis.* **2018**, *7*, 1000138.
- [4] Sadoff, C.W.; Borgomeo, E.; Uhlenbrook, S. Rethinking Water for SDG 6. *Nat. Sustain.* **2020**, *3*, 346–347.
- [5] Hanif, M.A.; Nadeem, F.; Zahid, M.; Khan, F.G.; Hanif, A.; Akhtar, M.N. Applications of Coagulation-Flocculation and Nanotechnology in Water Treatment. In *Aquananotechnology*; Elsevier, **2021**; pp. 523–548.
- [6] Garvasis, J.; Prasad, A.R.; Shamsheera, K.; Jaseela, P.; Joseph, A. Efficient Removal of Congo red from Aqueous Solutions Using Phyto-genic Aluminum Sulfate Nano Coagulant. *Mater. Chem. Phys.* **2020**, *251*, 123040.
- [7] Derouich, G.; Younssi, S.A.; Bennazha, J.; Cody, J.A.; Ouammou, M.; El Rhazi, M. Development of low-Cost Polypyrrole/Sintered Pozzolan Ultrafiltration Membrane and its Highly Efficient Performance for Congo red dye Removal. *J. Environ. Chem. Eng.* **2020**, *8*, 103809.
- [8] Schwarze, M.; Seo, D.; Bibouche, B.; Schomäcker, R. Comparison of Positively Charged Polymer Species and Cationic Surfactants for Methyl Orange Removal via Polyelectrolyte and Micellar Enhanced Ultrafiltration. *J. Water Proc. Eng.* **2020**, *36*, 101287.
- [9] Lahmar, H.; Benamira, M.; Douafer, S.; Messaadia, L.; Boudjerda, A.; Trari, M. Photocatalytic Degradation of Methyl Orange on the Novel Hetero-System La₂NiO₄/ZnO Under Solar Light. *Chem. Phys. Lett.* **2020**, *742*, 137132.
- [10] Jiang, R.; Zhu, H.-Y.; Fu, Y.-Q.; Jiang, S.-T.; Zong, E.-M.; Zhu, J.-Q.; Zhu, Y.-Y.; Chen, L.-F. Colloidal CdS Sensitized Nano-ZnO/Chitosan Hydrogel with Fast and Efficient Photocatalytic Removal of Congo Red Under Solar Light Irradiation. *Int. J. Biol. Macromol.* **2021**, *174*, 52–60.
- [11] Zheng, W.; Liu, Y.; Liu, W.; Ji, H.; Li, F.; Shen, C.; Fang, X.; Li, X.; Duan, X. A Novel Electrocatalytic Filtration System with Carbon Nanotube Supported Nanoscale Zerovalent Copper Toward Ultrafast Oxidation of Organic Pollutants. *Water Res.* **2021**, *194*, 116961.
- [12] Zhang, T.; Zhang, J.; Zou, D.; Cheng, F.; Su, R. A Promising Pd/Polyaniline/Foam Nickel Composite Electrode for Effectively Electrocatalytic Degradation of Methyl Orange in Wastewater. *Desalin. Water Treat.* **2020**, *189*, 386–394.
- [13] Peleyeju, M.G.; Mgedle, N.; Viljoen, E.L.; Scurr, M.S.; Ray, S.C. Irradiation of Fe–Mn@SiO₂ with Microwave Energy Enhanced its Fenton-Like Catalytic Activity for the Degradation of Methylene Blue. *Res. Chem. Intermed.* **2021**, 1–14.
- [14] Sidney Santana, C.; Freire Bonfim, D.P.; da Cruz, I.H.; da Silva Batista, M.; Fabiano, D.P. Fe₂O₃/MCM-41 as Catalysts for Methyl Orange Degradation by Fenton-Like Reactions. *Environ. Prog. Sustain. Ener.* **2021**, *40*, e13507.
- [15] Yuan, M.; Fu, X.; Yu, J.; Xu, Y.; Huang, J.; Li, Q.; Sun, D. Green Synthesized Iron Nanoparticles as Highly Efficient Fenton-Like Catalyst for Degradation of Dyes. *Chemosphere* **2020**, *261*, 127618.
- [16] Jia, Y.; Ding, L.; Ren, P.; Zhong, M.; Ma, J.; Fan, X. Performances and Mechanism of Methyl Orange and Congo red Adsorbed on the Magnetic ion-Exchange Resin. *J. Chem. Eng. Data* **2020**, *65*, 725–736.
- [17] Miao, J.; Zhao, X.; Zhang, Y.-X.; Lei, Z.-L.; Liu, Z.-H. Preparation of Hollow Hierarchical Porous CoMgAl-Borate LDH Ball-Flower and its Calcinated Product with Extraordinary Adsorption Capacity for Congo red and Methyl Orange. *Appl. Clay Sci.* **2021**, *207*, 106093.
- [18] Omorogie, M.O.; Babalola, J.O.; Unuabonah, E.I.; Gong, J.R. Clean Technology Approach for the Competitive Binding of Toxic Metal Ions Onto MnO₂ Nano-Bioextractant. *Clean Technol. Environ. Policy* **2016**, *18*, 171–184.
- [19] Pavithra, K.G.; Jaikumar, V. Removal of Colorants from Wastewater: A Review on Sources and Treatment Strategies. *J. Ind. Eng. Chem.* **2019**, *75*, 1–19.
- [20] Simonescu, C.M.; Tătăruș, A.; Culiță, D.C.; Stănică, N.; Ionescu, I.A.; Butoi, B.; Banici, A.-M. Comparative Study of CoFe₂O₄ Nanoparticles and CoFe₂O₄-Chitosan Composite for Congo Red and Methyl Orange Removal

- by Adsorption. *Nanomaterials* **2021**, *11*, 711.
- [21] Zheng, Y.; Cheng, B.; You, W.; Yu, J.; Ho, W. 3D Hierarchical Graphene Oxide-NiFe LDH Composite with Enhanced Adsorption Affinity to Congo red, Methyl Orange and Cr (VI) Ions. *J. Hazard. Mater.* **2019**, *369*, 214–225.
- [22] Abd El-Aziz, M.; Saber, E.; El-Khateeb, M. Preparation and Characterization of CMC/HA-NPs/Pulp Nanocomposites for the Removal of Heavy Metal Ions. *KGK-Kautschuk Gummi Kunststoffe* **2019**, *72*, 36–41.
- [23] Kumar, H.M.; Sangwan, P. Synthesis and Characterization of MnO₂ Nanoparticles Using Co Precipitation Technique. *Inter. J. Chem. Chem. Eng.* **2013**, *3*, 155–160.
- [24] Chen, W.-H.; Lu, K.-M.; Lee, W.-J.; Liu, S.-H.; Lin, T.-C. Non-oxidative and Oxidative Torrefaction Characterization and SEM Observations of Fibrous and Ligneous Biomass. *Appl. Energy* **2014**, *114*, 104–113.
- [25] Chen, W.-H.; Cheng, W.-Y.; Lu, K.-M.; Huang, Y.-P. An Evaluation on Improvement of Pulverized Biomass Property for Solid Fuel Through Torrefaction. *Appl. Energy* **2011**, *88*, 3636–3644.
- [26] Liu, Q.; Li, Y.; Chen, H.; Lu, J.; Yu, G.; Möslang, M.; Zhou, Y. Superior Adsorption Capacity of Functionalised Straw Adsorbent for Dyes and Heavy-Metal Ions. *J. Hazard. Mater.* **2020**, *382*, 121040.
- [27] Babalola, J.O.; Olayiwola, F.T.; Olowoyo, J.O.; Alabi, A.H.; Unuabonah, E.I.; Ofomaja, A.E.; Omorogie, M.O. Adsorption and Desorption Kinetics of Toxic Organic and Inorganic Ions Using an Indigenous Biomass: Terminalia Ivorensis Seed Waste. *Inter. J. Indust. Chem.* **2017**, *8*, 207–220.
- [28] Babalola, J.O.; Koiki, B.A.; Eniayewu, Y.; Salimonu, A.; Olowoyo, J.O.; Oninla, V.O.; Alabi, H.A.; Ofomaja, A.E.; Omorogie, M.O. Adsorption Efficacy of Cedrela Odorata Seed Waste for Dyes: Non Linear Fractal Kinetics and Non Linear Equilibrium Studies. *J. Environ. Chem. Eng.* **2016**, *4*, 3527–3536.
- [29] Freundlich, H. Over the Adsorption in Solution. *J. Phys. Chem.* **1906**, *57*, 1100–1107.
- [30] Langmuir, I. The Adsorption of Gases on Plane Surfaces of Glass, Mica and Platinum. *J. Am. Chem. Soc.* **1918**, *40*, 1361–1403.
- [31] Jeppu, G.P.; Clement, T.P. A Modified Langmuir-Freundlich Isotherm Model for Simulating pH-Dependent Adsorption Effects. *J. Contam. Hydrol.* **2012**, *129*, 46–53.
- [32] Ofomaja, A.E.; Naidoo, E.B.; Pholosi, A. Intraparticle Diffusion of Cr (VI) Through Biomass and Magnetite Coated Biomass: A Comparative Kinetic and Diffusion Study. *S. Afr. J. Chem. Eng.* **2020**, *32*, 39–55.
- [33] Babalola, J.O.; Olowoyo, J.O.; Durojaiye, A.O.; Olatunde, A.M.; Unuabonah, E.I.; Omorogie, M.O. Understanding the Removal and Regeneration Potentials of Biogenic Wastes for Toxic Metals and Organic Dyes. *J. Taiwan Instit. Chem. Eng.* **2016**, *58*, 490–499.
- [34] Babalola, J.O.; Bamidele, T.M.; Adeniji, E.A.; Odozi, N.W.; Olatunde, A.M.; Omorogie, M.O. Adsorptive Modelling of Toxic Cations and Ionic Dyes onto Cellulosic Extract. *Model. Earth. Syst. Environ.* **2016**, *2*, 1–15.
- [35] Wanyonyi, W.C.; Onyari, J.M.; Shiundu, P.M. Adsorption of Congo Red Dye from Aqueous Solutions Using Roots of Eichhornia Crassipes: Kinetic and Equilibrium Studies. *Ener. Procedia* **2014**, *50*, 862–869.
- [36] Tapan Kumar, S. Adsorption of Methyl Orange onto Chitosan from Aqueous Solution. *J. Water Resour. Protect.* **2010**, *2*(10), 1–9
- [37] Jalil, A.A.; Triwahyono, S.; Adam, S.H.; Rahim, N.D.; Aziz, M.A.A.; Hairon, N.H.H.; Razali, N.A.M.; Abidin, M.A.; Mohamadiah, M.K.A. Adsorption of Methyl Orange from Aqueous Solution onto Calcined Lapindo Volcanic Mud. *J. Hazard. Mater.* **2010**, *181*, 755–762.
- [38] Chen, S.; Zhang, J.; Zhang, C.; Yue, Q.; Li, Y.; Li, C. Equilibrium and Kinetic Studies of Methyl Orange and Methyl Violet Adsorption on Activated Carbon Derived from Phragmites Australis. *Desalination* **2010**, *252*, 149–156.
- [39] Zhu, H.; Jiang, R.; Fu, Y.-Q.; Jiang, J.-H.; Xiao, L.; Zeng, G.-M. Preparation, Characterization and Dye Adsorption Properties of γ -Fe₂O₃/SiO₂/Chitosan Composite. *Appl. Surf. Sci.* **2011**, *258*, 1337–1344.